Applications of high-resolution X-ray computed tomography in petrology, meteoritics and palaeontology

W. D. CARLSON, T. ROWE, R. A. KETCHAM & M. W. COLBERT

Department of Geological Sciences, University of Texas at Austin, Austin, Texas 78712, USA (e-mail: wcarlson@mail.utexas.edu)

Abstract: High-resolution and ultra-high-resolution X-ray computed tomography are rapid, non-destructive and extremely powerful techniques for three-dimensional examination and measurement of a great variety of geological materials and specimens with sizes from several millimetres to several decimetres. A review of recent applications in petrology, meteoritics and palaeontology, which utilized an instrument optimized for geological studies (High-Resolution X-ray Computed Tomography Facility of the University of Texas at Austin), documents an abundance of novel scientific results and illuminates the potential for still broader application of these techniques in the earth sciences.

Many earth science investigations require examination or measurement of the internal features of specimens in three dimensions, tasks to which X-ray computed tomography (CT) is well-suited. A variety of different X-ray CT instruments and techniques are available. The scale of the object to be studied and the spatial resolution required in the images commonly dictate which is employed (Table 1). High-resolution X-ray CT (HRXCT) and ultra-high-resolution X-ray CT (UHRXCT) are techniques suitable for studying objects with dimensions from a few millimetres to a few decimetres. Into this range of scales falls a wide variety of intriguing geological problems. This paper provides a selective review of recent HRXCT and UHRXCT work done at the University of Texas at Austin, in the form of very brief synopses of individual projects with references to the published literature for more complete exposition. Our purpose is to stimulate further exploitation of these techniques in the earth sciences by providing an overview of the broad range of geological questions that can be productively addressed using this rapid, non-destructive, visually powerful and fully digital tool.

Table 1. *General classification of X-ray computed tomography*

Type	Scale of observation	Scale of resolution
Conventional (medical)	m	mm
High-resolution	dm	100 μm
Ultra-high-resolution	cm	10 μm
Microtomography	mm	μm

Advantages of X-ray computed tomography for geological investigations

The best-known advantage of X-ray CT is its ability to quickly and non-destructively image the interior of opaque solid objects in three dimensions. For rare or irreplaceable specimens that cannot or should not be destructively sectioned – including most meteorites and many fossils – X-ray CT may be the only practical means of gaining information on internal materials and geometries or other features hidden from external view. Even if a specimen is regarded as expendable, X-ray CT eliminates the extreme laboriousness of serial sectioning.

The digital character of a CT dataset facilitates computer visualization and animation, allowing a user to interact with the data and to better understand the features and interrelationships among elements of the dataset. Similarly, digital data can be interrogated to quickly obtain quantitative measurements of dimensions, angles, volumes or nearly any metrical feature of interest. Finally, these digital data provide an unrivalled means of archiving and exchanging information. For example, few of the many palaeontologists interested in dinosaurs will ever have a chance to handle the skull of the world's oldest dinosaur, *Herrerasaurus* – only a single complete specimen is known and it resides in a museum in Argentina – but a high quality CT dataset provides unlimited virtual access, while offering information on its anatomy that is impossible to see even if one were holding the specimen in one's hands.

From: MEES, F., SWENNEN, R., VAN GEET, M. & JACOBS, P. (eds) 2003. *Applications of X-ray Computed Tomography in the Geosciences*. Geological Society, London, Special Publications, **215**, 7–22. 0305-8719/03/$15.

X-ray CT at the University of Texas at Austin

This article does not attempt to provide a comprehensive review of geological applications of HRXCT and UHRXCT in the published literature. Instead it focuses on selected projects conducted at the High-Resolution X-ray Computed Tomography Facility of the University of Texas at Austin, projects chosen to illustrate the wide range of geological objects and problems to which these techniques are applicable. Many projects in anthropology, biology, and engineering are likewise amenable to CT study, but these fields were considered to lie beyond the scope of this article.

The X-ray CT laboratory at the University of Texas is dedicated to applications in the geosciences and related fields. Because partial operational funding is provided by the US National Science Foundation, the laboratory functions as a national shared multi-user facility, welcoming external researchers. Most of the projects described below were undertaken in collaboration with colleagues from other institutions, as the cited literature clearly reflects.

The industrial scanner at the University of Texas was custom designed and built by Bio-Imaging Research, Inc., of Lincolnshire, Illinois. The principal design requirement was sufficient flexibility to provide imagery for a very broad range of geologic specimens and materials, that is, across a wide span of combinations of spatial resolution, density discrimination and penetrating ability. The objective was to produce an instrument that would complement existing facilities employing modified medical scanners (capable of penetrating specimens of moderate density, decimetres to metres in size, with spatial resolution on the order of a millimetre) and specialized facilities employing synchrotron radiation (capable of penetrating low- to moderate-density specimens, up to several millimetres in size, with spatial resolution on the order of a micrometre). This objective was met with a modular design that incorporates, within a single radiation-safety enclosure, two X-ray sources and three detectors. These sources and detectors can be used in various combinations to optimize trade-offs among penetrating ability, spatial resolution, density discrimination, imaging modes and scan times.

The scanner is comprised of two subsystems. One yields ultra-high-resolution data on small objects that can be penetrated by relatively low-energy X-rays. The other yields high-resolution data on larger or denser objects that can be penetrated only by higher-energy X-rays.

Ultra-high-resolution tomography of specimens up to a few cm in diameter employs a 200 kV micro-focal X-ray source, in combination with a specimen-positioning stage capable of $\sim$1 μm reproducibility in vertical positioning and a conventional medical image-intensifier detector. The system's primary magnification, which increases with the specimen's proximity to the X-ray source, combines with the fixed pixel size of the video image to determine the limits of spatial resolution. The great flexibility of this system allows imaging of specimens from several cm to a few mm in diameter with spatial resolution from *c.* 250 μm to as low as *c.* 5 μm in favourable cases.

High-resolution tomography of large specimens employs a 420 kV tungsten X-ray source, a rotating turntable that can accommodate samples up to 50 kg in weight and either of two available high-energy detectors. One detector is a 512-channel cadmium-tungstate solid-state linear array, which provides superior sensitivity because of its high absorption efficiency. Its vertical aperture (slice thickness) ranges from 5 mm down to 0.25 mm, with a horizontal channel pitch of 0.31 mm. The other high-energy detector is a 2048-channel gadolinium oxysulfide radiographic line scanner. This detector, although less sensitive, provides higher in-plane spatial resolution, with a channel pitch of 0.05 mm. It can be used either in a high-resolution mode, with a vertical aperture of 0.25 mm, or (by sacrificing some sensitivity) in a thick-slice, rapid-scan mode using a vertical aperture that can vary from 0.5 to 5 mm. Operating in translate-rotate mode, the high-energy subsystem can image specimens up to 500 mm in diameter. The source and detectors are capable of 750 mm of vertical motion, but the unobstructed sample volume is 1500 mm tall, so specimens up to a metre and a half in maximum dimension (e.g. segments of drill cores) can be scanned by first imaging one half, then inverting the specimen to scan the other half. At the opposite end of the size spectrum, this subsystem can also be used to scan any smaller specimen for which *c.* 250 μm spatial resolution is sufficient.

Adding to the flexibility of this scanner is its ability to acquire data in several different modes, to further optimize performance trade-offs. Both subsystems can collect data in third-generation geometry (rotate-only, centred and variably offset) and the high-energy subsystem can also be operated in second-generation geometry (translate-rotate), which allows for increased resolution within subvolumes of the specimen by selective reconstruction of the raw absorption data. On both subsystems, complete control over the positioning of the specimen ensures that the maximum magnification (hence, maximum resolution) can always be achieved. A 'multi-slice'

mode on the ultra-high-resolution subsystem permits simultaneous acquisition of data for a central slice and several neighbouring slices above and below. This markedly reduces scan times at a small cost in data quality owing to slight off-axis distortion. This distortion is caused in part by utilization of standard filtered back-projection reconstruction, which assumes all data are coplanar. A 'cone-beam' imaging mode, using the Feldkamp reconstruction algorithm, is also implemented on the ultra-high-resolution subsystem. This allows simultaneous collection of data throughout the full 3D volume of small specimens, further reducing scan times for applications in which maximal resolution and dimensional accuracy are not required.

Contrast resolution in CT images depends on the differential X-ray attenuation characteristics of the phases present, which are complex functions of X-ray energy, mass density and composition. Using the lower-energy X-rays on the UHRXCT system, which provides greater sentivity to differences in atomic number, it is possible to differentiate phases with virtually identical mass densities, such as quartz and orthoclase (cf. Fig. 4 in Ketcham & Carlson 2001).

Additional background information about X-ray CT methods applied to geological materials and further details of image acquisition, optimization and interpretation, are presented elsewhere (Ketcham & Carlson 2001).

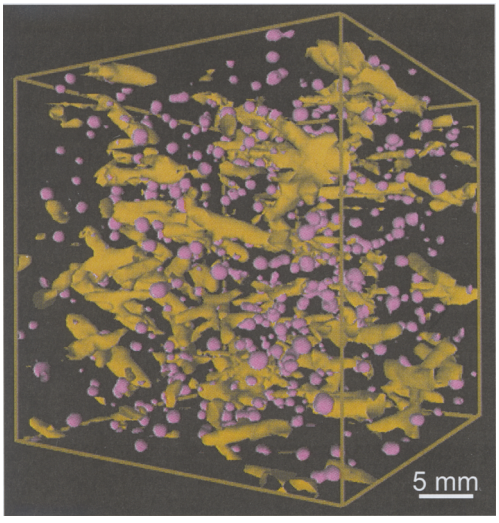

Fig. 1. Isosurface image of garnet (rendered violet) and staurolite (rendered yellow-brown) in pelitic schist from Picuris Mountains, New Mexico. Bounding box for image is approximately $45 \times 45 \times 42$ mm.

Applications in petrology

Most of the applications in this section exploit the digital character of X-ray CT data, which makes it practical to obtain precise quantitative measurements of the proportions, shapes, sizes and locations of particles, crystals, segregations or voids. Because such measurements are commonly numbered in the thousands or even tens of thousands, it is possible with such data to succeed with statistical analyses that would be otherwise impractical, if not impossible, to undertake.

Quantitative analysis of metamorphic textures

Three-dimensional CT data on the sizes and locations of crystals (Fig. 1) permit discrimination between competing hypotheses for the atomic-scale mechanisms controlling the growth of porphyroblasts. Early work demonstrated that reaction kinetics limited by rates of intergranular diffusion were common for garnet in regionally metamorphosed rocks (Carlson & Denison 1992; Denison & Carlson 1997; Denison *et al.* 1997). Numerical simulations of such processes, constrained by the X-ray CT data, allowed first-ever estimates of key kinetic parameters such as the absolute rates of garnet nucleation and intergranular diffusion of aluminium (the species whose transport is rate-limiting) (Carlson *et al.* 1995). Compositional studies based on serial-sectioning guided by X-ray CT data (Chernoff & Carlson 1997, 1999) demonstrated the importance of this reaction control: sluggish intergranular diffusion appears to account for the observation that in some metamorphic rocks, Ca and many trace elements fail to equilibrate at the thin-section scale during garnet growth, severely restricting the confidence that can be placed in thermobarometric methods that assume otherwise. X-ray CT data made possible a statistical analysis of textures in a prograde sequence of garnetiferous pelites, which revealed that increases in grain size and decreases in crystal number densities are principally the consequence of higher nucleation temperatures, rather than the result of post-crystallization annealing (Carlson 1999; Hirsch & Carlson 2001).

Metasomatism in Earth's mantle and the origin of diamonds

The character of mantle metasomatism and the origin of diamonds – fundamental enigmas in mantle petrology – have been addressed by complete three-dimensional characterization of

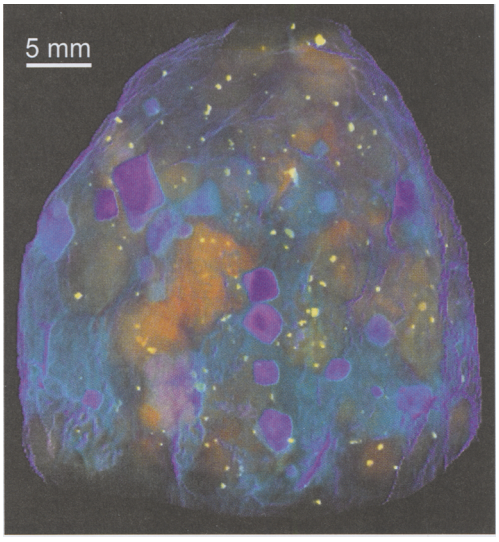

Fig. 2. Three-dimensional reconstruction from X-ray CT data of a diamondiferous eclogite from Udachnaya, Siberia, approximately 35 mm in diameter. Matrix of partially altered clinopyroxene has been rendered semi-transparent in shades of green; large crystals of garnet are semi-transparent in shades of red-orange; diamonds are opaque in shades of blue to violet; sulfides are yellow and the outer surface of the specimen is semi-transparent in shades of blue. Specimen courtesy of Lawrence Taylor, University of Tennessee, Knoxville.

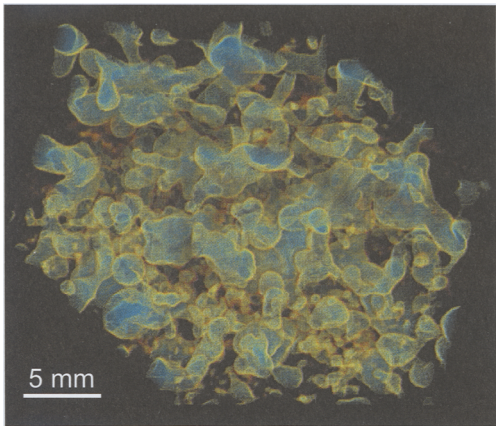

Fig. 3. Three-dimensional reconstruction from X-ray CT data of a 15 mm cube of vesicular basalt. Vesicle boundaries have been rendered semi-transparent in shades of green to yellow. Volumes of such irregular vesicles cannot be determined accurately by any two-dimensional sectioning technique, but are rapidly computed from X-ray CT imagery. Specimen courtesy of Dork Sahagian, University of New Hampshire. Reprinted from Carlson *et al.* (1999), with permission.

textural relationships in extraordinary diamondiferous eclogites from Udachnaya, Siberia (Taylor *et al.* 2000). CT imagery revealed that none of the diamonds were enclosed within either garnet or clinopyroxene, but instead all were spatially associated with 3D networks of subplanar zones of altered clinopyroxene that penetrate the specimens (Fig. 2). The implication is that the diamond post-dates formation of the eclogitic assemblage and that it was introduced into the rock in conjunction with metasomatic input(s) of carbon-rich fluids.

Palaeoaltimetry and continental uplift from size distributions of basalt vesicles

Differences in the modal vesicle sizes of samples from the bottom and top of basaltic lava flows preserve a quantitative record of palaeoelevations at the time of eruption (Sahagian & Maus 1994). When vesicles are nearly spherical, modal vesicle sizes in three dimensions can be recovered by laborious stereological techniques in thin section, but deformation or coalescence of bubbles in the melt renders stereology erroneous and requires collection of true three-dimensional data (Fig. 3). Such data are acquired easily, rapidly and accurately by means of X-ray CT (Proussevitch *et al.* 1998). When combined with geochronology on the flows, determinations of palaeoelevation yield quantitative rates of continental uplift. Application of this technique to basaltic lavas of the SW USA has defined the timing and extent of uplift of the Colorado Plateau (Sahagian *et al.* 2002).

Topology of melt flow paths in migmatites

Processes and rates of melt flow in the anatectic zone depend on several factors related to the geometry and topology of the flow paths. CT imagery of leucosome-melanosome-mesosome relationships in migmatites (Fig. 4) can be used to make quantitative determinations of features relevant to the permeability of such rocks to melt. This includes the effective porosity, ratios of pore surface to volume, mean pore radius, surface roughness and the connectivity and tortuosity of flow paths. The leucosome network geometry of two contrasting migmatites has been determined by X-ray CT and serial sectioning (Brown *et al.* 1999). This analysis demonstrated the 3D connectivity of leucosome in both samples, highlighted differences between the two in effective porosity and tortuosity, and provided constraints on flow-path topology that can be used in quantitative models simulating melt flow.

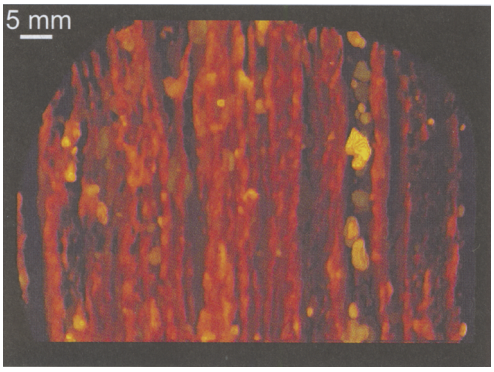

Fig. 4. Three-dimensional reconstruction from X-ray CT data of stromatic migmatite from southern Brittany, France (maximum dimension 63 mm). Leucosome has been rendered mostly transparent; melanosome and mesosome are shown as opaque in reddish shades and garnet crystals are rendered opaque in shades of yellow. Specimen courtesy of Michael Brown and Mary Anne Brown, University of Maryland. Reprinted from Brown *et al.* (1999), with permission.

Magmatic differentiation from crystal-mush compaction

The recent discovery that plagioclase crystals cluster together to form a continuous 3D network early in the crystallization history of slowly cooled basaltic magma (Philpotts *et al.* 1998) offers a means of determining the degree of the compaction of cooling flows and thus permits evaluation of this potential mechanism for their chemical differentiation. Measurements from thin sections and CT data (Fig. 5) on the thick Holyoke flood basalt of Connecticut (USA) revealed a pattern of chain compaction and dilation that matches exactly the pattern indicated by the chemical variation in this flow (Philpotts *et al.* 1999). The origin of these networks in the upper solidification front of the flow, combined with their preservation in lower parts of the flow, is clear evidence for convective transfer of dense crystal mush from the roof to the floor of the magma sheet, a mechanism long postulated but previously never unequivocally demonstrated (Philpotts & Dickson 2000).

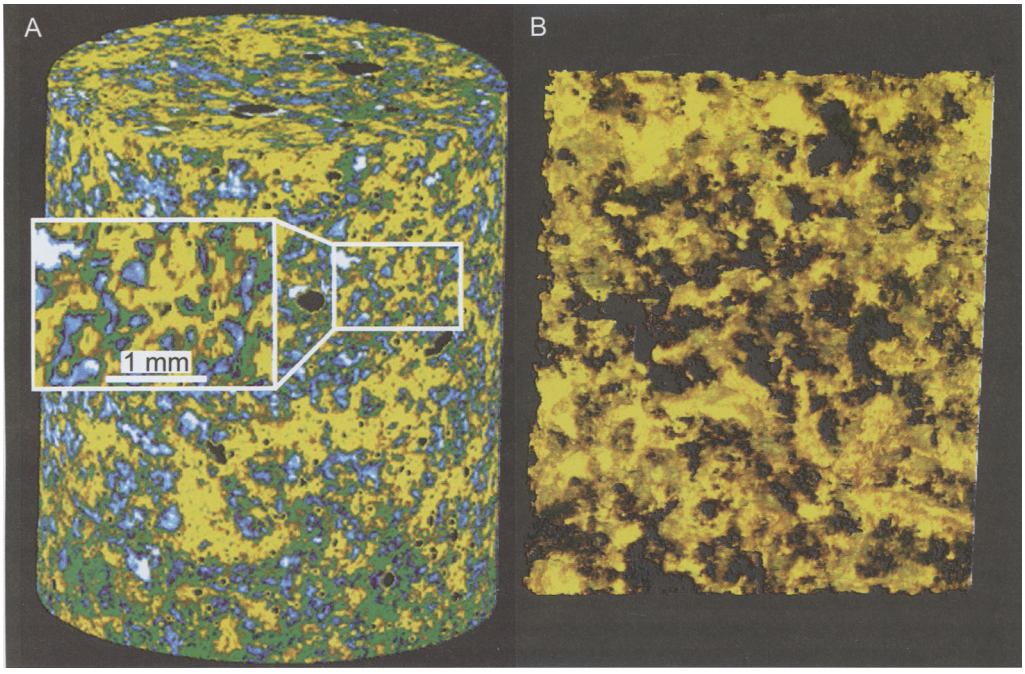

Fig. 5. **(a)** Three-dimensional reconstruction from X-ray CT data of a 1 cm tall core of Holyoke basalt subjected to 50% partial melting. Plagioclase is rendered yellow, pyroxene is blue-to-white, glass is green, and voids are black. **(b)** Three-dimensional reconstruction of subsampled region, in the shape of a thin slab from the centre of the core, with all components except plagioclase rendered transparent. Specimen courtesy of Anthony Philpotts, University of Connecticut. Reprinted from Philpotts *et al.* (1999), with permission.

Modelling of fluid flow through vuggy pore space

Medical CT data has been employed extensively to determine porosity and permeability and to visualize fluid flow in sediments and core specimens (Wellington & Vinegar 1987; Withjack 1988; Withjack & Akervoll 1988). However, in some cases the flow characteristics of reservoir lithologies are dominated by large-scale features, such as fractures or vugs, that make them impossible to analyse either with medical CT or traditional flow methods because the size of sample required to adequately represent these features is too large. Industrial CT scanners that use higher-energy X-rays are able to image larger and denser samples, allowing flow properties to be studied and modelled effectively in many cases. In one such study, high-resolution CT of a 28×36 cm caprinid reef block from the Pipe Creek Formation in Texas revealed that the vuggy porosity caused by rudist fossils was highly but not completely connected (Fig. 6). Computer models based on the CT data indicate high effective permeability, poor sweep efficiency and large anisotropy, all caused by the large but tortuous fluid pathways.

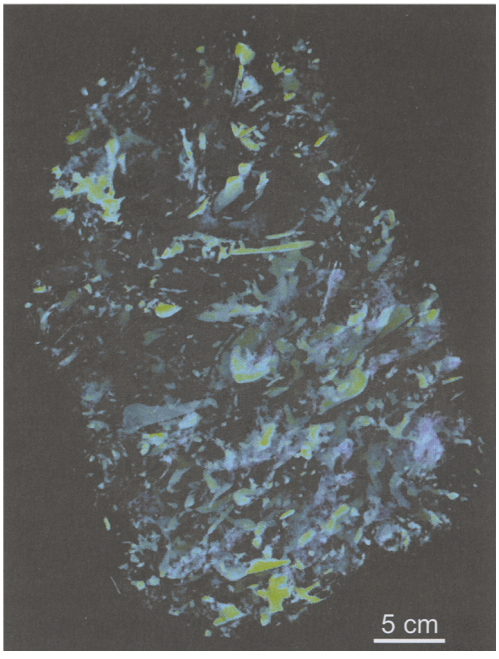

Fig. 6. Three-dimensional reconstruction from X-ray CT data of porosity dominated by rudist fossils in a large block (28 cm diameter, 36 cm high) of 'Pipe Creek Reef', a caprinid build-up in the Albian-aged Glen Rose Formation, Texas. Green shades indicate air-filled vugs and blues represent vugs with mud infilling, in addition to smaller-scale macroporosity. Specimen courtesy of James Jennings, University of Texas at Austin Bureau of Economic Geology.

Applications in meteoritics

Because of the extreme rarity of meteorites, destructive analysis of them is avoided whenever possible. For these precious specimens, X-ray CT permits imaging of three-dimensional relationships that are otherwise unobservable. The applications presented in this section exploit this ability of X-ray CT to reveal internal features non-destructively, as well as its ability to quantify proportions of materials and to measure particle volumes.

Melt generation, segregation and migration in lodranites

Initial curatorial slabbing of the lodranite meteorite GRA95209 produced the surprising discovery of abundant metal segregated from the mixed silicate-metal matrix. X-ray CT revealed a sheath of metal (obscured by fusion crust) extending along the exterior surface of much of the specimen and into the interior, where it connected to several veins and stringers of metal within the matrix. The matrix was seen to include metal-poor silicate-rich regions. The coalescing veins and dykelets revealed in 3D by X-ray CT (Fig. 7) are readily interpreted as pathways of melt migration, and measurements from CT data of the relative volumes of metal and the metal-depleted matrix permit mass-balance calculations that rule out a completely local origin for the melt (Carlson & McCoy 1998; McCoy & Carlson 1998). The images, therefore, record a complicated and intriguing picture of melt generation and migration in the lodranite parent body, a primitive planetisimal that is one of the best existing models for processes occurring during core-mantle segregation in the terrestrial planets.

Impact-induced melting and metamorphism of chondrites

Veinlets of metal apparent on the exterior surface of the Portales Valley meteorite prompted a CT study to determine the textural character of metal-silicate relationships and to guide curatorial efforts at cutting the meteorite for distribution to scientists for research purposes. The scans revealed that the specimen was strongly brecciated, with metal filling the interstices between angular

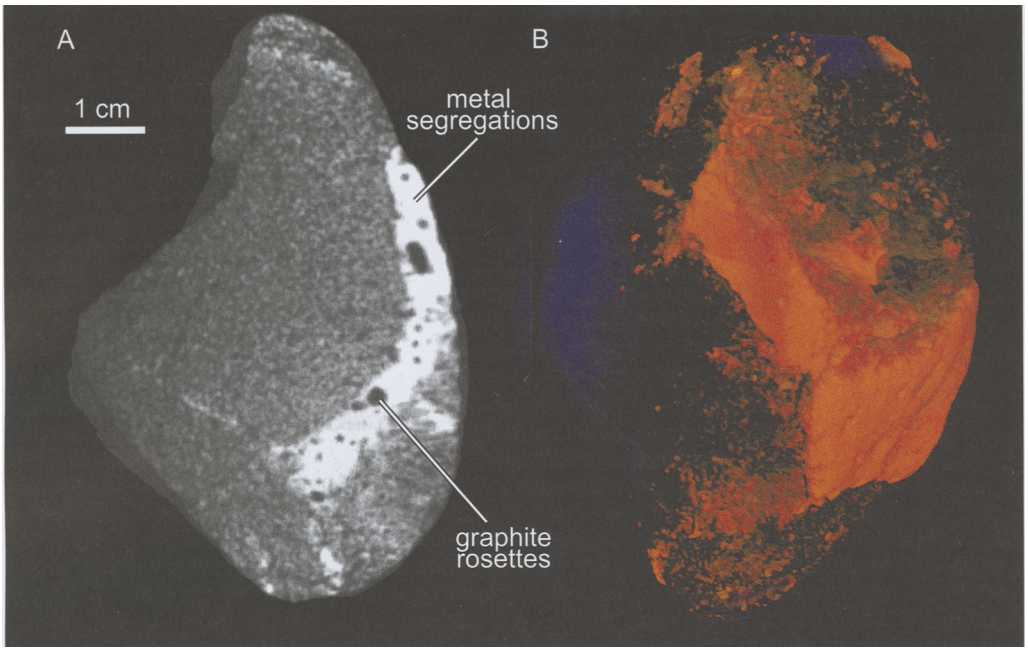

Fig. 7. (**a**) Perspective view of X-ray CT images of lodranite meteorite GRA95209 (maximum dimension *c.* 72 mm), producing a 'virtual sawcut' through the specimen exposing its internal features. Homogeneous bright regions are metal segregations; they contain dark, roughly spherical spots identified optically as rosettes of graphite. Mottled regions contain mixture of fine-grained metal and silicates, in varying proportions as expressed by overall grey-scale level. (**b**) Three-dimensional volume rendering of the same data to show the distribution of metal. Metal particles are rendered opaque in shades of orange; all other materials are nearly transparent in shades of dark blue. Specimen courtesy of Timothy McCoy, Smithsonian Institution, and Marilyn Lindstrom, NASA-Johnson Space Center. Reprinted from Carlson & McCoy (1998), with permission.

silicate clasts (Fig. 8). Subsequent study suggested an origin for this chondrite in which metamorphism, metal fusion and brecciation resulted from impact. The CT data suggest the possibility of size grading of the silicate clasts within larger pockets of metal, which requires the presence of an appreciable gravity field, implying that the impact likely took place while the specimen was part of its parent body (Rubin *et al.* 2001).

Particle sorting in the solar nebula

Particle sizes in chondritic meteorites potentially contain information on turbulence and sorting processes in the solar nebula. Hypotheses that differentiate between mass sorting in a quiescent nebula and aerodynamic sorting in a turbulent nebula can be tested if the sizes of both chondrules and metal-troilite particles can be measured. Although chondrules may be equant enough to allow size determination by stereological methods in thin-section, metal-troilite particles are so irregularly shaped that their true volumes cannot be recovered from any sectional measurement (Fig. 9). A high-resolution X-ray CT study of particle sizes in three different meteorites (Kuebler *et al.* 1999) provided key data regarding the processes of particle sorting in the solar nebula. Because in all three cases the metal-troilite particles, in comparison to the chondrules, have different masses but similar aerodynamic stopping times, these data are supportive of a model involving accretion in eddies in a turbulent solar nebula.

Applications in palaeontology

The rarity of many fossils, combined with their morphological complexity, makes them ideal candidates for examination using X-ray CT. Many of the applications in this section benefit principally from the ability to digitally manipulate X-ray CT data for enhanced visualization, although the ability to non-destructively examine features hidden from external view and to make precise morphological measurements are also prominent advantages to palaeontological applications.

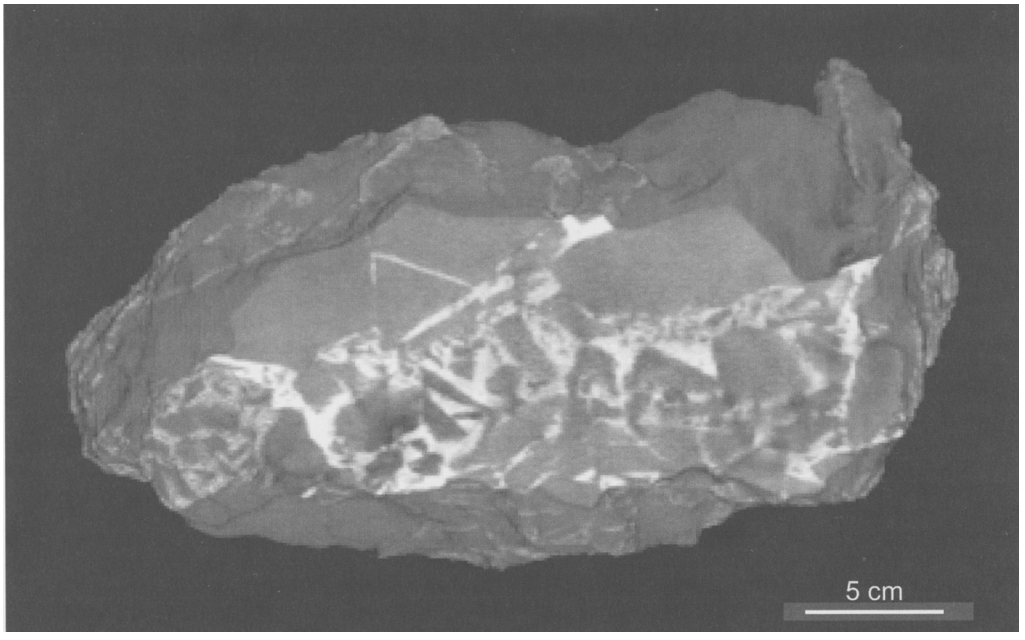

Fig. 8. 'Virtual sawcut' through Portales Valley meteorite (maximum dimension ~30 cm) produced by creating a perspective view of CT images. Brightest whites (metal) lie in the planar surface of the page, and the surrounding material in darker shades is a rendering of the exterior surface below that level. Small silicate particles (grey) in the wider portions of the metallic region tend to concentrate near the 'top' of the metal veins, suggesting segregation in a gravity field (oriented vertically in this image). Specimen courtesy of John Wasson and Alan Rubin, University of California, Los Angeles. Reprinted from Rubin *et al.* (2001), with permission.

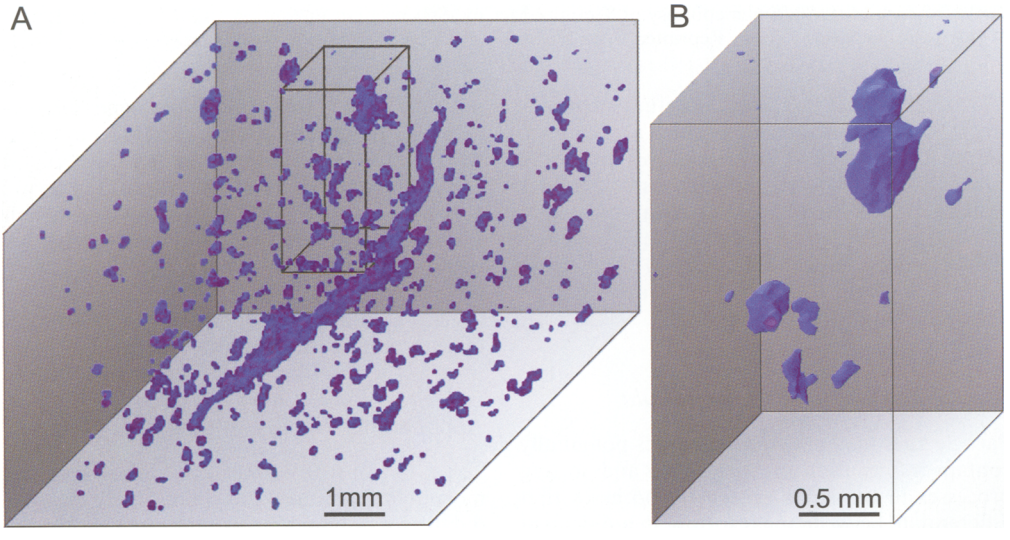

Fig. 9. Three-dimensional representation of shapes, sizes and positions of metal-troilite particles in Hammond Downs chondritic meteorite from X-ray CT data. (**a**) Particles in cubic volume roughly 7 mm on edge include one extraordinarily large vein-like object; dashed prism locates volume shown in part (**b**) of this figure. (**b**) Enlargement of a portion of same dataset, emphasizing that the irregular shapes of these grains make it impossible to determine their volumes accurately by any two-dimensional sectioning method. Specimen courtesy of Harry McSween, Jr, University of Tennessee, Knoxville. Reprinted from Kuebler *et al.* (1999), with permission.

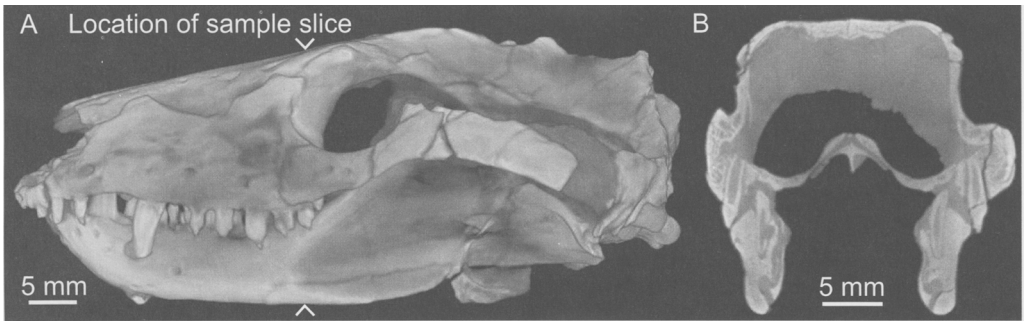

Fig. 10. (**a**) Three-dimensional reconstruction from X-ray CT data of the Early Triassic fossil skull of *Thrinaxodon* (maximum dimension 7.2 cm). (**b**) Single data slice illustrating the complex internal structures that can be imaged by UHRXCT. Bright areas are fossilised bone, darker areas are the silicate matrix. Specimen courtesy of the University of California Museum of Paleontology (UCMP #40466), University of California at Berkeley.

Mammalian origins: the endocranium of Thrinaxodon

The first application of HRXCT to palaeontology was the scanning of a 280 million-year-old fossilized skull of a distant mammalian relative known as *Thrinaxodon* (Fig. 10), an animal that has been at the centre of many studies of early mammalian evolution (e.g. Kemp 1982; Gauthier *et al.* 1988; Rowe 1988, 1993). Early mammalian history is principally represented by tiny animals, and their fossils are very rare and scattered widely among collections (Rowe 1999). *Thrinaxodon* is one of the larger species, being the size of a house cat, and it is known from only a handful of specimens. Non-destructive examination of *Thrinaxodon* using CT imagery was aimed at answering several long-standing problems surrounding the origin of mammals by extracting new information on the internal structure of the skull and on the size and morphology of the brain as recorded in its endocast. This work offered the first look at the endocranial cavity and permitted the first digital endocast of a specimen to be extracted from a digital dataset (Rowe *et al.* 1993).

Mammalian origins: the neocortex

The modern marsupial *Monodelphis domestica*, a popular lab opossum that grows to the size of a rat, is one of the least specialized of living mammals and its brain, compared to its body size, is one of the smallest of any living mammal (Fig. 11). Scanning a growth series of skulls allowed measurement of endocranial volume throughout life, revealing how the brain and skull affect each other as they grow. Comparisons of *Monodelphis* with *Thrinaxodon* and several other fossils showed that the origin of Mammalia (Rowe 1988) coincided with the appearance of the neocortex, a hugely inflated part of the forebrain that is unique to mammals. A consequence of this great cerebral expansion was enhancement of the senses of smell and hearing, heightened motor-sensory integration and probably also an increased basal metabolic rate (Rowe 1996*a*, *b*).

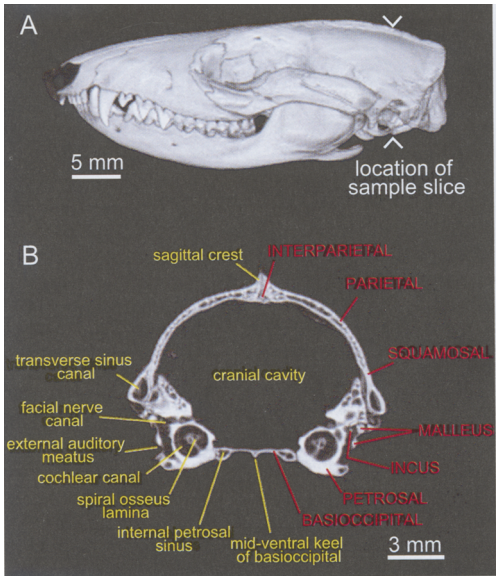

Fig. 11. (**a**) Three-dimensional volumetric reconstruction from X-ray CT data of the skull of the extant opossum *Monodelphis domestica* (maximum dimension 4.0 cm). (**b**) Individual CT slice with structures labelled to show the richness of detail obtainable by UHRXCT, even on very small specimens. Specimen courtesy of the Vertebrate Paleontology Laboratory, University of Texas at Austin.

Mammalian origins: the middle ear

Comparisons of *Monodelphis* and *Thrinaxodon* to other fossils revealed that an inflation in brain volume causes profound remodelling at the back of the skull, which answered one of the oldest problems in mammalian origins. Mammals are distinctive in having three separate bones that conduct sound through the middle ear. Other vertebrates with a sound-transducing ear have only a single middle ear bone. In these species, the homologs of the extra two mammalian middle ear bones remain as parts of the lower jaw. How the bones of the mammalian middle ear became detached from the jaw and repositioned to their definitive mammalian configuration was considered highly problematic. Measurements from the CT data (Fig. 12) demonstrated that different relative growth of the brain and ear ossicles – both in early mammalian evolution and during early development in living species – is responsible for the trajectory and direction of movement of the ear ossicles (Rowe 1996*a*, *b*).

Jaws of fossil marsupials: tooth replacement, reproductive patterns, taxonomy

UHRXCT imagery of an 80-million-year-old fossil jaw of *Alphadon* provided the first evidence of tooth replacement in a Mesozoic marsupial (Cifelli *et al.* 1996) and demonstrated that the modern pattern of marsupial tooth replacement is very ancient. Correlations between tooth development and reproductive pattern permitted further inferences regarding the antiquity of the

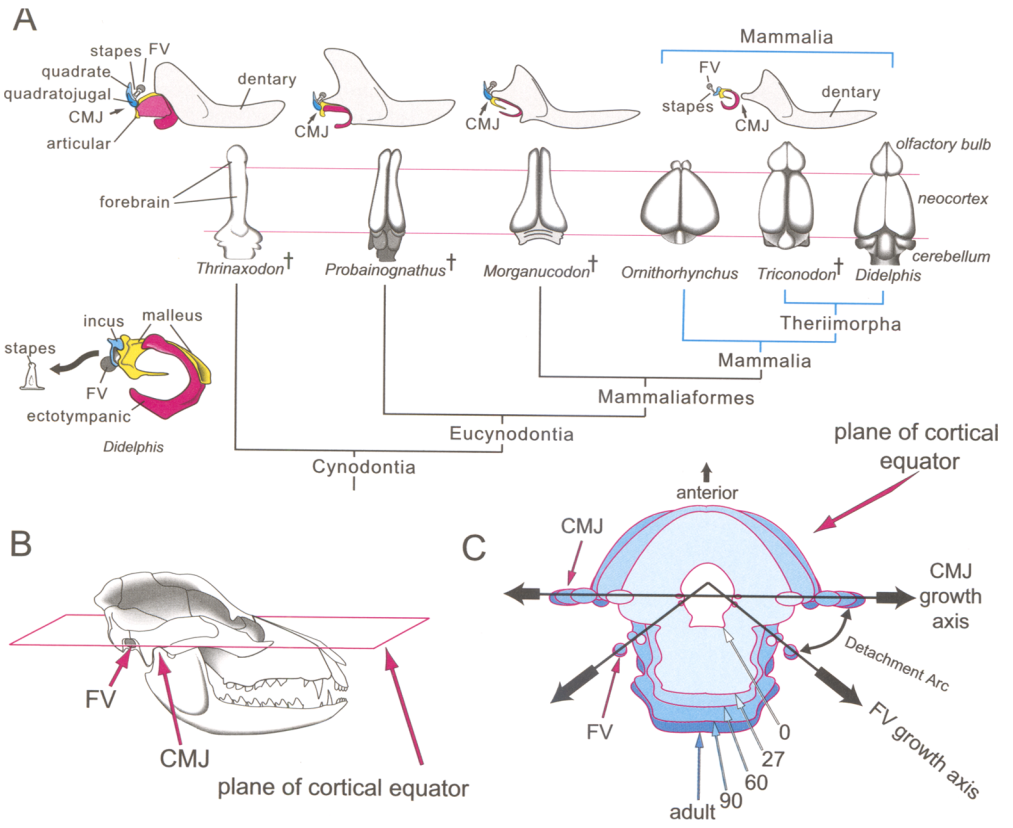

Fig. 12. (**a**) Co-evolution of the mammalian mandible and middle ear (in right lateral view) and the brain (illustrated by dorsal views of endocasts), plotted together on a phylogeny of selected mammals and their closest extinct relatives (Gauthier *et al.* 1988; Rowe 1988, 1993). Abbreviations: CMJ – craniomandibular joint; FV – fenestra vestibuli of inner ear. (**b**) Location of cortical equator on didelphid skull. (**c**) Superimposed projections of cortical equator, from X-ray CT imaging of *Monodelphis domestica*, showing the increase in equatorial circumference with age. Divergent trajectories of the CMJ and FV growth axes define an *arc of detachment* whose growth leads to detachment and caudal displacement of the auditory chain. Reprinted from Rowe (1996*b*), with permission.

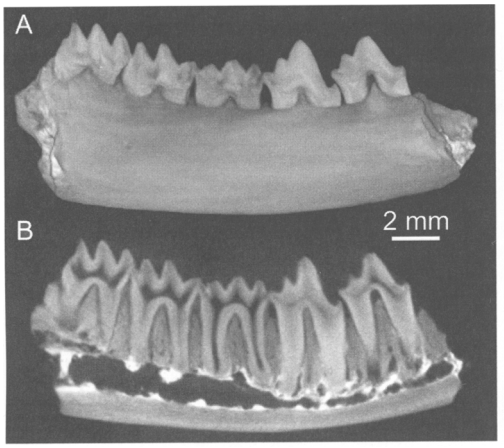

Fig. 13. The lower jaw of *Arundelconodon*, a Late Cretaceous marsupial from the eastern seaboard of the United States (19.3 mm length). **(a)** Three-dimensional volumetric rendering from X-ray CT data. **(b)** A sample CT slice, demonstrating that this specimen retains the primitive condition of non-interlocked tooth roots (Cifelli *et al.* 1999). Specimen courtesy of the Smithsonian Institution, National Museum of Natural History. Reprinted from Cifelli *et al.* (1999), with permission.

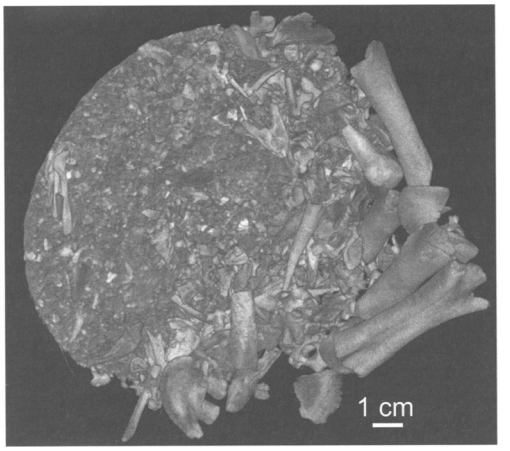

Fig. 14. Three-dimensional volumetric rendering from X-ray CT data of the embryonic remains contained inside an intact egg of *Aepyornis maximus*, the elephant bird (maximum dimension 15.2 cm). Specimen courtesy of the National Geographic Society.

distinctive marsupial reproductive patterns. Successful analysis of this tiny jaw prompted other high-resolution CT studies of tiny Mesozoic fossils (Cifelli & de Muizon 1998; Cifelli *et al.* 1999). In another study, UHRXCT aided in the description of *Arundelconodon*, a new species of Mesozoic mammal known only from a tiny jaw (Cifelli *et al.* 1999), by revealing otherwise unavailable information on taxonomically important aspects of the structure of its tooth roots (Fig. 13).

Elephant bird

HRXCT has successfully imaged the embryo of the extinct elephant bird of Madagascar, *Aepyornis maximus* (Weintraub 2000). The elephant bird was the largest bird known, weighing roughly 440 kg and standing nearly 4 m tall (Amadon 1947), and it laid the largest eggs ever discovered. Although it became extinct in historic times, only a few intact eggs are known. Conventional X-radiography revealed the presence of an embryo in at least one of them (Wetmore 1967), but the imagery provided no useful information on its skeletal structure. HRXCT scanning of a complete egg revealed details of the embryonic skeleton; image processing of the CT dataset permitted digital 'extraction' of the disarticulated embryo from the egg (Fig. 14). Detailed analysis is still underway (Balanoff 2001).

Forensic palaeontology: identifying forgeries

HRXCT data provide unique criteria by which to judge the authenticity of fossils. A high-profile example is '*Archaeoraptor*', which *National Geographic* magazine had heralded as a 'missing link' between birds and extinct dinosaurs (Sloan 1999). Analysis of the CT data revealed that the forgery (Fig. 15) had been assembled from at least two, and perhaps as many as five, different specimens and species (Rowe *et al.* 2001).

Mammalian cranial architecture: visualizing cranial cavities

X-ray CT makes it possible to non-destructively examine and measure the interior cavities of vertebrate skulls (Brochu 2000; Marino *et al.* 2000; Colbert 2001; Franzosa 2001; Maisey 2001). These cavities are typically hidden from external view and are difficult or impossible to study by traditional means. They include not only the endocranial cavity that houses the brain and related structures, but also sinus cavities, inner ear labyrinths or any non-bony space. While it has long been recognized that endocranial casts provide a close representation of mammalian brain morphology, the architectural relationship between the brain, sinus cavities and overall cranial shape has been difficult to evaluate. The

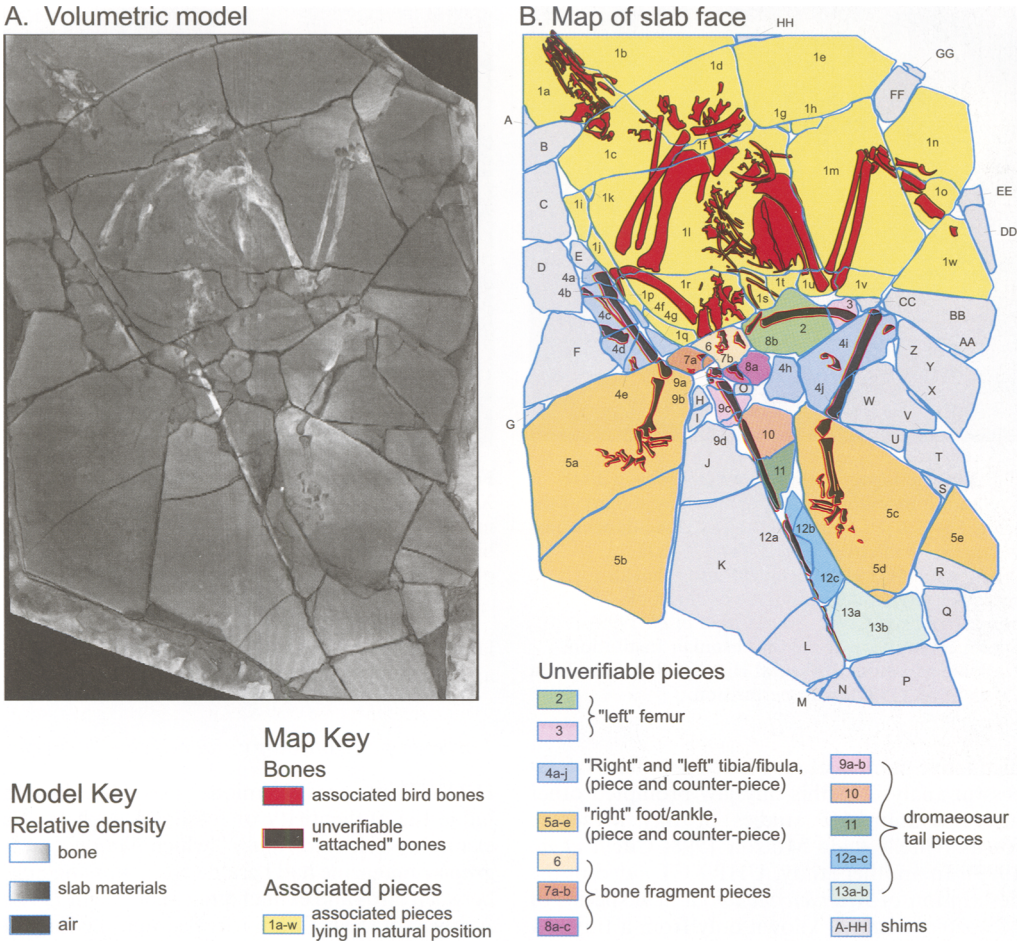

Fig. 15. Two computer-generated models of the face of the *Archaeoraptor* slab as it was presented for X-ray CT scanning (27 cm width). The specimen was scanned from top to bottom in planes perpendicular to this view. **(a)** Volumetric model generated from superimposed CT slices. **(b)** Map of the slab face, colour-coded to indicate the nature of the associations between its 88 constituent pieces. Reprinted from Rowe *et al.* (2001), with permission.

changing architectural contribution of these cavities to skull morphology during evolution was revealed by a series of CT scans of extant tapirs and of a new fossil tapiroid from the Middle Eocene of North America (Colbert 1999). Comparison of CT-based endocasts reveals that the unique posterior 'telescoping' of the skull of Recent tapirs is also accompanied by the development of enlarged frontal sinuses that surround the olfactory bulbs and frontal lobes of the brain and that accounts for the elevation of the frontal bones (Fig. 16). These sinuses are not present in the new Eocene fossil tapiroid, which also lacks elevated frontals, an indication of the importance of these sinuses in the overall architecture of the skull.

Non-destructive examination of fossils in amber

Insects and other small animals trapped in amber provide a rare glimpse of the 'in-life' morphology of ancient fauna. Attempts to extract such specimens from their encasement are inevitably destructive. Although such specimens can often be examined productively using microscopy and photography, ultra-high-resolution CT has proven useful for some more difficult cases (Grimaldi *et al.* 2000). In one case, the surface morphology of a scorpion (*Arthropoda: Buthidae*) was extracted from a specimen in which the amber was too clouded for standard light-based techniques (Fig. 17). In another, the skeleton of a

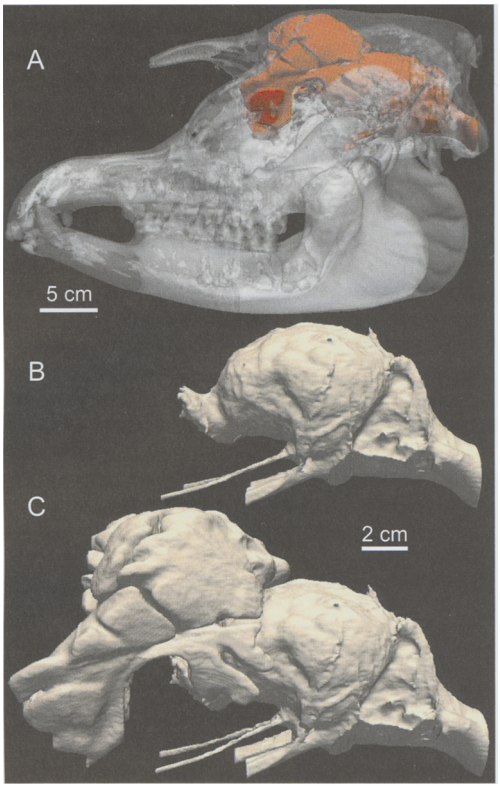

Fig. 16. Skull and endocasts of the Malayan Tapir (*Tapirus indicus*) rendered from X-ray CT data. Maximum dimension of skull is 42 cm. **(a)** Relationship of the sinus cavity and endocranial cavity to the exterior of the cranium. Cavities rendered in red, bone in semitransparent white. **(b)** Cranial cavity endocast. **(c)** Relationship of the sinus endocast to the cranial cavity endocast, showing that the frontal sinus surrounds much of the anterior endocranial cavity. Specimen courtesy of American Museum of Natural History.

Sphaerodactylus gecko, which was otherwise obscured by the skin, was sufficiently preserved to permit a number of morphological elements to be identified and extracted, allowing comparison with more commonplace fossilized material.

Structural elements responsible for density banding in scleractinian corals

Density bands that form annually in some corals are a valuable tool for reconstructing past environmental and climatic conditions, because they allow isotopic analysis of material precipitated at known times in the past. Better understanding

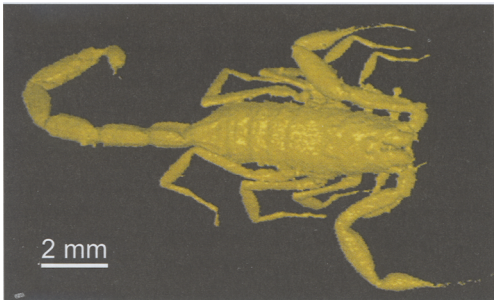

Fig. 17. Three-dimensional rendering from X-ray CT data of the remains of a scorpion trapped in Miocene-aged Dominican amber. Optical examination of this specimen was impossible because of the opacity of the amber in which it was embedded. Specimen courtesy of David Grimaldi, American Museum of Natural History.

of these data and considerable additional detail may be available if the skeletal elements responsible for banding can be identified, which may then be related to specific organismal processes. X-radiographs have long been used to reveal density banding within a skeletal slab, but they provide insufficient detail to examine the underlying structures. High-resolution X-ray CT imagery of

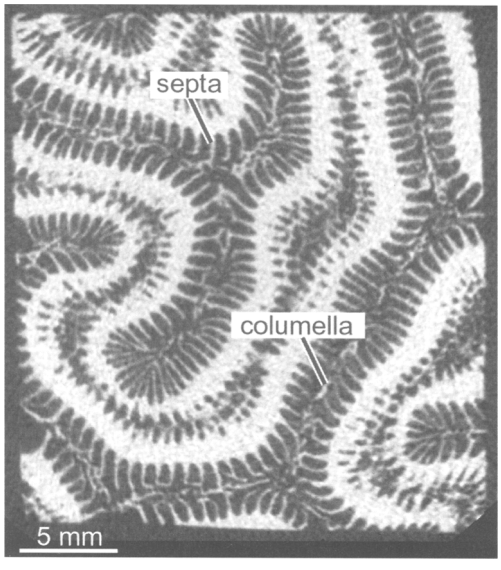

Fig. 18. High-resolution X-ray CT image of the coral *Diploria strigosa* (edge length 25 mm), revealing annual density bands that are associated with enlargement of the thinner structural elements (septa and columella) in the image. Specimen courtesy of Richard Dodge and Kevin Helmle, Nova Southeastern University.

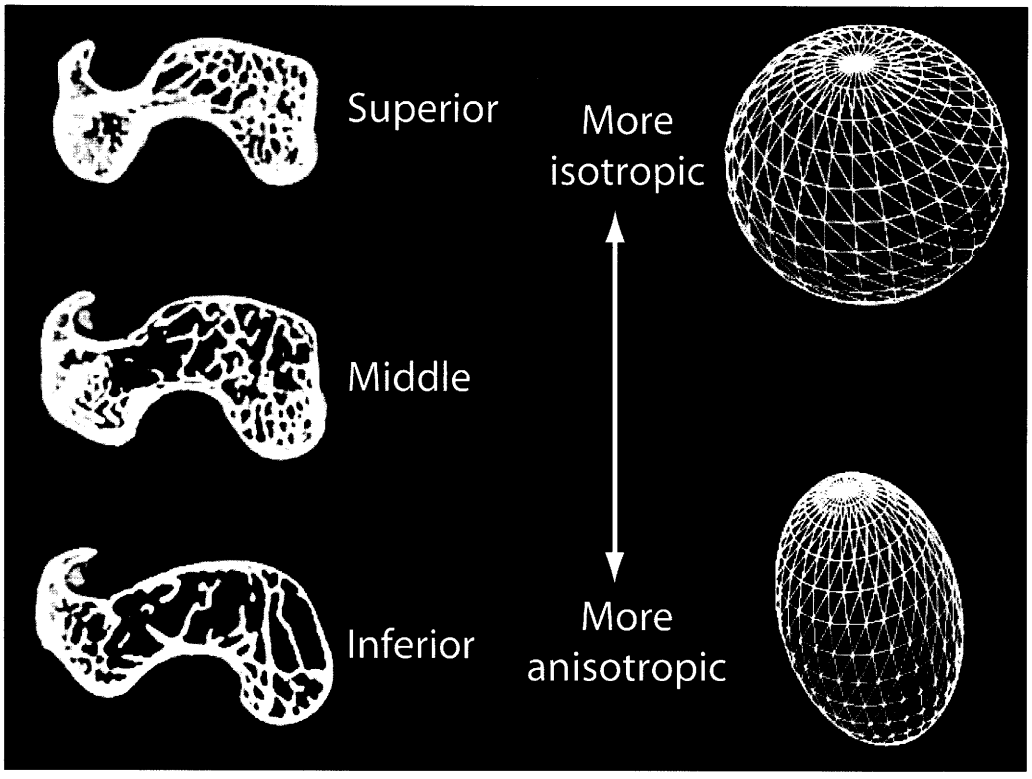

Fig. 19. X-ray CT images of trabecular bone of the femoral head of *Galago senegalensis* (maximum dimension 10 mm) with ellipsoidal representations of the degree of anisotropy of the three-dimensional trabecular structure. Anisotropy increases with increasing distance from the superior end of the bone. Specimen courtesy of the Smithsonian Institution, National Museum of Natural History.

the coral *Diploria strigosa* (Fig. 18) reveals that density bands in this species are associated with thickening of septal and columellar structures (Helmle *et al.* in press).

Trabecular architecture in primates as an indicator of locomotor patterns

It has been hypothesized for over 100 years that trabecular bone plays an important structural role in the musculoskeletal system of animals and that it dynamically responds to applied loads through growth. High-resolution X-ray CT data permit quantitative determination of the architecture of trabecular bone near limb joints in small primates through determination of bone volume fraction and a fabric tensor that indicates the material principal axes and degree of anisotropy (Fig. 19). A systematic study of the trabecular bone in femoral heads of Recent small primates shows that significant differences exist between leaping and non-leaping species, with the former having relatively anisotropic bone (Ryan 2000; Ryan & Ketcham 2002). These results for extant primates permit inferences about the locomotor patterns of extinct species to be drawn from fossil specimens in which trabecular bone patterns are preserved.

Conclusions

The advent of high-resolution and ultra-high-resolution instruments has opened up a wide realm of new applications of X-ray CT to geological problems. Given the advantages of these techniques – their speed, their non-destructive character and their ability to produce data in a digital form that facilitates visualization and quantification – one should expect only further expansion of applications into an even wider range of fields in the coming years. The projects selected for inclusion in this review are indicative

of much of the technique's potential, but the full range of possibilities – which remains largely unexplored – is surely as diverse as the geological sciences are broad.

The authors acknowledge, with gratitude, the support of the W. M. Keck Foundation and the Geology Foundation of the University of Texas at Austin, who together with the US National Science Foundation (NSF EAR-9406258) made possible the initial purchase of our CT scanner. We are also grateful for continued support of the facility's operational costs by the US National Science Foundation (NSF EAR-9816020 and NSF EAR-0004082). C. Denison played a significant role in data acquisition and image processing for several of the projects included in this review.

References

AMADON, D. 1947. An estimated weight of the largest known bird. *The Condor*, **49**, 159–165.

BALANOFF, A.M. 2001. Unscrambling the egg: digital extraction of an elephant bird (*Aepyornis*) embryo from an intact egg. *Journal of Vertebrate Paleontology*, **21 (suppl. to No. 3)**, 31A.

BROCHU, C.A. 2000. A digitally rendered endocast for *Tyrannosaurus rex*. *Journal of Vertebrate Paleontology*, **20**, 1–6.

BROWN, M.A., BROWN, M., CARLSON, W.D. & DENISON, C. 1999. Topology of syntectonic melt flow networks in the deep crust: inferences from three-dimensional images of leucosome geometry in migmatites. *American Mineralogist*, **84**, 1793–1818.

CARLSON, W.D. 1999. The case against Ostwald ripening of porphyroblasts. *Canadian Mineralogist*, **37**, 403–413.

CARLSON, W.D. & DENISON, C. 1992. Mechanisms of porphyroblast crystallization: results from high-resolution computed X-ray tomography. *Science*, **257**, 1236–1239.

CARLSON, W.D., DENISON, C. & KETCHAM, R.A. 1995. Controls on the nucleation and growth of porphyroblasts: Kinetics from natural textures and numerical models. *Geological Journal*, **30**, 207–225.

CARLSON, W.D., DENISON, C. & KETCHAM, R.A. 1999. High-resolution X-ray computed tomography as a tool for visualization and quantitative analysis of igneous textures in three dimensions. *Electronic Geosciences*, **4**, 3.

CARLSON, W.D. & MCCOY, T.J. 1998. High-resolution X-ray computed tomography of lodranite GRA 95209. Lunar and Planetary Science XXIX, Abstract #1541, Lunar and Planetary Institute, Houston (CD-ROM).

CHERNOFF, C.B. & CARLSON, W.D. 1997. Disequilibrium for Ca during growth of pelitic garnet. *Journal of Metamorphic Geology*, **15**, 421–438.

CHERNOFF, C.B. & CARLSON, W.D. 1999. Trace-element zoning as a record of chemical disequilib rium during garnet growth. *Geology*, **27**, 555–558.

CIFELLI, R.L. & DE MUIZON, C. 1998. Marsupial mammal from the Upper Cretaceous North Horn Formation, central Utah. *Journal of Paleontology*, **72**, 532–537.

CIFELLI, R.L., LIPKA, T.R., SCHAFF, C.R. & ROWE, T.B. 1999. First Early Cretaceous mammal from the eastern seaboard of the United States. *Journal of Vertebrate Paleontology*, **19** 199–203.

CIFELLI, R.L., ROWE, T., LUCKETT, W.P., BANTA, J., REYES, R. & HOWES, R.I. 1996. Fossil evidence for the origin of the marsupial pattern of tooth replacement. *Nature*, **379**, 715–718.

COLBERT, M.W. 1999. *Patterns of evolution and variation in the Tapiroidea (Mammalia, Perissodactyla)*. PhD thesis, University of Texas at Austin.

COLBERT, M.W. 2001. Digital visualization of cranial cavities: examples from fossil and recent mammals. *Journal of Vertebrate Paleontology*, **21 (suppl. to No. 3)**, 41A.

DENISON, C. & CARLSON, W.D. 1997. Three-dimensional quantitative textural analysis of metamorphic rocks using high-resolution computed X-ray tomography. Part II: application to natural samples. *Journal of Metamorphic Geology*, **15**, 45–57.

DENISON, C., CARLSON, W.D. & KETCHAM, R. 1997. Three-dimensional quantitative textural analysis of metamorphic rocks using high-resolution computed X-ray tomography. Part I: methods and techniques. *Journal of Metamorphic Geology*, **15**, 29–44.

FRANZOSA, J.W. 2001. Constructing digital endocasts of theropods using a high-resolution X-ray computed tomography scanner. *Journal of Vertebrate Paleontology*, **21 (suppl. to No. 3)**, 51A.

GAUTHIER, J., KLUGE, A.G. & ROWE, T. 1988. Amniote phylogeny and the importance of fossils. *Cladistics*, **4**, 105–209.

GRIMALDI, D., NGUYEN, T. & KETCHAM, R. 2000. Ultra-high-resolution X-ray computed tomography (UHR CT) and the study of fossils in amber. *In*: GRIMALDI, D. (ed.) *Studies on Fossils in Amber, with Particular Reference to the Cretaceous of New Jersey*. Backhuys, Leiden, 77–91.

HELMLE, K.P., DODGE, R.E. & KETCHAM, R.A. 2003. Skeletal architecture and density banding in *Diploria strigosa* by X-ray computed tomography. *In*: *Proceedings of the 9th International Coral Reef Symposium*, 365–372.

HIRSCH, D.M. & CARLSON, W.D. 2001. Causes of variation in textures along a regional metamorphic field gradient (abstr.). *In*: *Eleventh Annual V.M. Goldschmidt Conference*, Abstract #3203, (CD-ROM).

KEMP, T.S. 1982. *Mammal-like Reptiles and the Origin of Mammals*. Academic Press, London.

KETCHAM, R.A. & CARLSON, W.D. 2001. Acquisition, optimization and interpretation of X-ray computed tomographic imagery: applications to the geosciences. *Computers & Geosciences*, **27**, 381–400.

KUEBLER, K.E., MCSWEEN, H.Y., JR, CARLSON, W.D. & HIRSCH, D.M. 1999. Sizes and masses of chondrules and metal-troilite grains in ordinary chondrites. *Icarus*, **141**, 96–106.

MAISEY, J.G. 2001. Stone deaf? CT scanning and low frequency phonoreception in extinct sharks. *Journal of Vertebrate Paleontology*, **21 (suppl. to No. 3)**, 51A.

MARINO, L., UHEN, M.D., FROHLICH, B., ALDAG, J.M., BLANE, C., BOHASKA, D. & WHITMORE, F.C., JR. 2000. Endocranial volume of mid-late Eocene archeocetes (Order: Cetacea) revealed by computed tomography: Implications for cetacean brain evolution. *Journal of Mammalian Evolution*, **7**, 81–94.

MCCOY, T.J. & CARLSON, W.D. 1998. Opaque minerals in the GRA 95209 lodranite: a snapshot of metal segregation. Lunar and Planetary Science XXIX, Abstract #1675, Lunar and Planetary Institute, Houston (CD-ROM).

PHILPOTTS, A.R., BRUSTMAN, C.M., SHI, J., CARLSON, W.D. & DENISON, C. 1999. Plagioclase chain networks in slowly cooled basaltic magma. *American Mineralogist*, **84**, 1819–1829.

PHILPOTTS, A.R. & DICKSON, L.D. 2000. The formation of plagioclase chains during convective transfer in basaltic magma. *Nature*, **406**, 59–61.

PHILPOTTS, A.R., SHI, J. & BRUSTMAN, C.M. 1998. Role of plagioclase crystal chains in the differentiation of partly crystallized basaltic magma. *Nature*, **395**, 343–346.

PROUSSEVITCH, A., KETCHAM, R.A., CARLSON, W.D. & SAHAGIAN, D. 1998. Preliminary results of X-ray CT analysis of Hawaiian vesicular basalts. *EOS*, **79**, 360.

ROWE, T. 1988. Definition, diagnosis and origin of Mammalia. *Journal of Vertebrate Paleontology*, **8**, 241–264.

ROWE, T. 1993. Phylogenetic systematics and the early history of mammals. *In*: SZALAY, F.S., NOVACEK, M.J. & MCKENNA, M.C. (eds) *Mammalian Phylogeny*. Springer Verlag, New York, 129–145.

ROWE, T. 1996*a*. Brain heterochrony and evolution of the mammalian middle ear. *In*: GHISELIN, M. & PINNA, G. (eds), *New Perspectives on the History of Life*. California Academy of Sciences Memoir **20**, 71–96.

ROWE, T. 1996*b*. Coevolution of the mammalian middle ear and neocortex. *Science*, **273**, 651–654.

ROWE, T. 1999. At the roots of the mammalian tree. *Nature*, **398**, 283–284.

ROWE, T., CARLSON, W.D. & BOTTORFF, W. 1993. *Thrinaxodon*: Digital Atlas of the Skull [CD-ROM]. University of Texas Press.

ROWE, T., KETCHAM, R., DENISON, C., COLBERT, M., XU, X. & CURRIE, P.J. 2001. The *Archaeoraptor* forgery. *Nature*, **410**, 539–540.

RUBIN, A.E., ULFF-MOLLER, F., WASSON, J.T. & CARLSON, W.D. 2001. The Portales Valley meteorite breccia: evidence for impact-induced melting and metamorphism of an ordinary chondrite. *Geochimica et Cosmochimica Acta*, **65**, 323–342.

RYAN, T. 2000. Quantitative analysis of trabecular bone structure in the femur of lorisoid primates using high-resolution X-ray computed tomography (abstr). *American Journal of Physical Anthropology*, **Suppl. 30**, 266–267.

RYAN, T.M. & KETCHAM, R.A. 2002. The three-dimensional structure of trabecular bone in the femoral head of strepsirrhine primates. *Journal of Human Evolution*, **43**, 1–26.

SAHAGIAN, D., PROUSSEVITCH, A. & CARLSON, W. 2002. Timing of Colorado Plateau uplift: initial constraints from vesicular basalt-derived paleoelevations. *Geology*, **50**, 807–810.

SAHAGIAN, D.L. & MAUS, J.E. 1994. Basalt vesicularity as a measure of atmospheric pressure and paleoelevation. *Nature*, **372**, 449–451.

SLOAN, C.P. 1999. Feathers for *T. Rex*? New birdlike fossils are missing links in dinosaur evolution. *National Geographic*, **196**, 98–107.

TAYLOR, L.A., KELLER, R.A., SNYDER, G.A., WANG, W., CARLSON, W.D., HAURI, E.H., MCCANDLESS, T., KIM, K.R., SOBOLEV, N.V. & BEZBORODOV, S.M. 2000. Diamonds and their mineral inclusions, and what they tell us: a detailed 'pull-apart' of a diamondiferous eclogite. *International Geology Review*, **42**, 959–983.

WEINTRAUB, B. 2000. New 'pictures' of a giant bird. *National Geographic*, **198**, viii.

WELLINGTON, S.L. & VINEGAR, H.J. 1987. X-ray Computerized Tomography. *Journal of Petroleum Technology*, 885–898.

WETMORE, A. 1967. Recreating Madagascar's giant extinct bird. *National Geographic*, **132**, 488–493.

WITHJACK, E.M. 1988. Computed tomography for rock property determination and fluid flow visualization. *Society of Petroleum Engineers Formation Evaluation*, **3**, 696–704.

WITHJACK, E.M. & AKERVOLL, I. 1988. Computed tomography studies of 3-D miscible displacement behavior in a laboratory five-spot model. *In*: *Proceedings of the Society of Petroleum Engineers Annual Technical Conference and Exhibition, Houston, Texas, 2–5 October*, Paper **SPE 18095**.